Magnetic γ-Fe$_2$O$_3$ Loaded Attapulgite Sorbent for Hg^0 Removal in Coal-fired Flue Gas

Lu Dong[1,2], Yaji Huang[1]*, Hao Chen[1], Lingqin Liu[1], Changqi Liu[1], Ligang Xu[1],

Jianrui Zha[1], Yongxing Wang[1], Hao Liu[2]*

[1]Key Laboratory of Energy Thermal Conversion and Control of Ministry of Education, School of Energy and Environment, Southeast University, Nanjing 210096, China

[2] Faculty of Engineering, University of Nottingham, University Park, Nottingham, NG7 2RD, England, UK

Corresponding authors

 *Yaji Huang, heyyj@seu.edu.cn

*Hao Liu, liu.hao@nottingham.ac.uk

Keywords: Magnetic sorbent, Attapulgite, Element mercury removal, Coal-fired flue gas

Abstract

A magnetically recoverable composite mercury removal sorbent was produced by introducing magnetic γ-Fe$_2$O$_3$ into attapulgite (ATT) (xFe1ATT) via coprecipitation

1

method and used to remove Hg^0 in the simulated coal-fired power plant flue gas. The as-prepared 0.5Fe1ATT sorbent was characterized by XRD, BET, TEM, VSM, XPS and FTIR analyses. The results showed that the Hg^0 removal performance of the composite of γ-Fe_2O_3 and ATT was significantly promoted compared to the pure γ-Fe_2O_3 and ATT individually. A relatively high magnetization value and good Hg^0 removal performance were obtained by the sample of 0.5Fe1ATT. O_2 could enhance Hg^0 removal activity via the Mars-Maessen mechanism. NO displayed a significant promotion effect on Hg^0 removal as a result of the formation of active species like NO_2 and NO^+. SO_2 inhibited the removal of Hg^0 due to its competition adsorption against Hg^0 for the active sites and the sulfation of the sorbent. However, the introduction of NO could obviously alleviate the adverse effect of SO_2 on the Hg^0 removal capability. H_2O showed a prohibitive effect on Hg^0 removal due to its competition with Hg^0 for the active sites. The findings of this study is of fundamental importance to the development of efficient and economic magnetic mercury sorbents for Hg^0 removal from coal-fired boiler flue gases.

1 Introduction

Mercury pollution has attracted worldwide attention due to the properties of extreme toxicity, high volatility and strong bioaccumulation of mercury compounds in the environment [1, 2]. Coal-fired power plants have been regarded as the main anthropogenic source of mercury emissions [3] and almost account for one third of the total mercury emission caused by human activities [4]. Mercury Treaty Negotiations were approved by

the United Nations Environment Programme (UNEP) at the UNEP 25th GC Session for the control of mercury [5]. The mercury species emitted from coal-fired boiler flue gases exist in three forms: the elemental mercury (Hg^0), the oxidized mercury (Hg^{2+}), and particulate-bound mercury (Hg^p) [6, 7]. Hg^{2+} is water soluble and can be effectively removed by wet flue gas desulfurization (WFGD) [8]. Hg^p can be easily collected by particulate control devices (PCD) [9, 10]. However, Hg^0 is extremely hard to be captured by existing air pollution control devices (APCDs) due to its high volatility and low solubility in water [11]. Hence, it is imperative to develop efficient technologies to remove Hg^0. Many methods have been developed for the control of mercury emissions from coal-fired boiler flue gases. By far, the injection of a sorbent upstream of the PCD to remove Hg^0 from coal-fired boiler flue gases has been the most commonly used technology [12]. Among the various kinds of sorbents that applied to remove Hg^0, activated carbon (AC) is widely considered as an effective mercury sorbent, which can be ascribed to its developed pore structure, large specific surface area, and abundant surface oxygen functional groups. Activated carbon injection (ACI) has been widely used to remove Hg^0 from coal-fired power plant flue gases. However, a high operating cost is incurred with ACI as AC can only be used once. Furthermore, after capturing mercury, the AC sorbents are normally collected by particulate devices together with fly ash and this leads to an increase in carbon content of the fly ash and the contamination of the fly ash by the captured mercury, negatively affecting the commercial utilization of fly ash and hence impeding the application of ACI [13, 14]. To

3

alleviate these problems, many researchers have investigated the use of non-carbon based sorbents, including calcium based sorbents [15], metal and metal oxides based sorbents [16, 17], metal–organic framework based sorbents [18] and fly ashes [19] in recent years. Ghorishi investigated the simultaneous removal ability of Hg^0, SO_2, and NOx using oxidized Ca-based sorbents and found the mercury sorption capacity of these sorbents was comparable to that of the commercial AC [15]. Sun et al. have found that silver loaded 4A zeolite has a superiority Hg^0 removal efficiency and capacity due to the fact that mercury can react with the active sites by Ag-Hg amalgamation [20]. Manganese oxide [21, 22], cerium oxide [23], iron oxide [24], and copper oxide [25] based sorbents have always showed great Hg^0 removal ability due to the oxidation of Hg^0 to Hg^{2+} by the high valance metal ion and abundant chemisorption oxygen and lattice oxygen species on the surface of these sorbents. However, the mercury removal sorbents mentioned above are relatively expensive and therefore other cost-effective mercury sorbents, such as clay materials which have been commonly applied as promising and cheap catalyst supports [26, 27] , must be found if they are to be used to remove mercury from coal-fired boiler flue gases.

Attapulgite (also called palygorskite) is an environmentally friendly hydrated magnesium aluminum silicate natural mineral clay with chain layered crystal structures which can be widely found around the world [28, 29]. Attapulgite (ATT) with a very low price of only 15-20 USD/ton, is abundant in China, although, more than 60% of the national deposits are located in Xuyi County, Jiangsu Province [30]. ATT has been

considered to be an ideal natural catalyst support exhibiting excellent activity and chemical adsorption property due to its large specific surface and unique microporous structure [31]. In addition, the surface of ATT can be used as a nucleation center to stabilize nanoparticles, leading to the formation of a uniform metal compound /ATT nano-composite [32, 33]. There are increasing research efforts focusing on the modification of ATT as a catalyst for the selective catalytic reduction (SCR) of NOx in recent years [33-35]. However, few have investigated Hg^0 removal from coal-fired boiler flue gases by using ATT. Although the palygorskite impregnated with $CuCl_2$ and $CuBr_2$ has been used as a Hg^0 removal sorbent and resulted in a significant enhancement of the mercury removal ability after modification [36], it faces the same problems as an AC sorbent, i.e. the cost of the one-time injection of the sorbent is too high and the mercury-laden sorbent cannot be separated from the fly ash, hence leading to the contamination of fly ash. Thus, it is imperative to develop a feasible approach to separate the mercury-captured sorbent from fly ash. The magnetic material, such as maghemite (γ-Fe_2O_3) can be introduced to sorbents to separate them effectively by an external magnetic field [37]. The combination of magnetic material and ATT for the application of water pollution removal has been verified as a promising way to recover the ATT particles from aqueous solutions [38, 39]. To the authors' knowledge, the related research on the combination of magnetic medium and ATT for mercury removal has not been reported so far in the literature.

In the present work, the magnetic ATT composite was first synthesized through the co-precipitation method, and then applied as the mercury sorbent to investigate the Hg^0 removal performance in a fixed-bed reactor set-up. The effects of the magnetic medium/ATT loading mass ratio, reaction temperature, and flue gas composition on the Hg^0 removal efficiency were studied. The main objectives of this study were to conduct a preliminary assessment of mercury removal from the simulated coal-fired flue gas by magnetic ATT composite sorbents and to find adsorbents with excellent recovery performance and high mercury removal efficiency. The results of this research can provide further insight into the development and application of cost-effective magnetic sorbents for mercury removal from coal-fired boiler flue gases.

2 Experimental

2.1 Preparation of magnetic ATT sorbent

The raw mineral attapulgite was obtained from Dingbang Co. (Changzhou, China) and other chemical reagents used in this study were obtained from Sinopharm Chemical Reagent Co., Ltd (Shanghai, China) in analytical grade.

The preparation procedure for the magnetic ATT composite is as follows. The raw ATT was first pretreated with deionized water to wash off the surface soluble impurities. Then the obtained ATT was dispersed in deionized water to form dispersed slurry under vigorously stirring conditions and the required amounts of $FeCl_2$ and $FeCl_3$ (with a mole ratio of Fe^{2+}/Fe^{3+} of 1:2) were added to the ATT dispersion. Further, the $NH_3 \cdot H_2O$ solution was dropwise added into the iron chloride ATT mixed solution under

6

vigorously stirring conditions until the pH value reached about 9. The dispersion was kept being stirred at 60 $^{\circ}$C for 3 h. After that, the sediment was centrifuged and washed thoroughly with deionized water and ethanol for several times. Finally, the sample was dried at 100 $^{\circ}$C for 10 h, followed by calcination at 250 $^{\circ}$C for 4 h under air atmosphere to obtain the γ-Fe$_2$O$_3$/ATT composites. The pure γ-Fe$_2$O$_3$ was prepared by the same method without the addition of ATT. The γ-Fe$_2$O$_3$/ATT composites are denoted as xFe1ATT, where Fe represents γ-Fe$_2$O$_3$, ATT represents attapulgite, and x represents the mass ratio between γ-Fe$_2$O$_3$ and ATT. The values of x was fixed at 0, 0.2, 0.5, and 1, respectively. 'x=0' represents the raw pure ATT which was dried and calcined under the same condition as that of xFe1ATT composites. The preparation of the xFe1ATT samples is illustrated in Fig. 1.
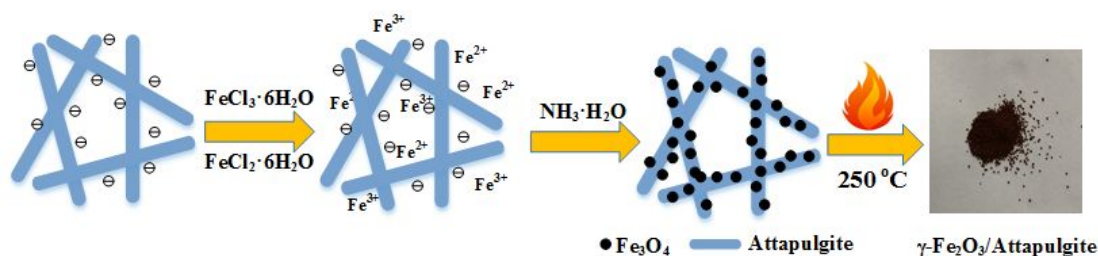

Fig. 1 Schematic of the synthesis of magnetic attapulgite composites.

2.2 Characterization of sorbent

The crystal structure of the prepared samples was identified by a powder X-ray diffraction (XRD) with a XD-3 X-ray diffractometer using Cu Kα radiation in the range of 10°-80° at room temperature. The micrograph structure of the sorbents was analyzed by transmission electron microscopy (TEM) (JEM-2100, JEOL, Japan). The BET

specific surface area (SSA) and pore structure of the sorbents were obtained by N_2 adsorption-desorption in a constant volume adsorption apparatus (Gold APP) at the liquid-nitrogen temperature of 77 K. The magnetism of the magnetic samples was determined by a physical property measurement system with a vibrating sample magnetometer (Lakeshore, VSM). The XPS measurements were acquired by a K-α spectrometer (ESCALAB 250XI, Thermo, US) at room temperature under ultra-high vacuum. All binding energies of the samples were calibrated using the reference carbon (C 1s) peak at 284.8 eV. The surface groups of the samples were determined by Fourier-transform infrared (FTIR) spectra (IS10, Thermo, US). Mercury temperature programmed desorption (TPD) tests were carried out as follows: after the Hg^0 adsorption at 150 °C for 90 min over 0.5Fe1ATT under different reaction conditions, the mercury loaded sample was purged with N_2 at 35 °C for at least 30 min in order to make sure the outlet mercury concentration was below $1\mu g/m^3$, then the sample was heated from 35 °C to 680 °C at heating rate of 10 °C /min.

2.3 Experimental apparatus

The evaluation of mercury removal ability with different sorbents was performed in a fixed bed flow quartz reactor (Fig. 2). The compressed gas cylinders comprised of N_2, O_2, NO, and SO_2 were used to provide different gas components for the simulated coal-fired boiler flue gas. The total flow rate of the simulated flue gas was precisely controlled to be 2 L/min by mass flow controllers. The micro-injection pump was used

8

to inject water into the Teflon tube which was wrapped with heating lining and heated to 110 $^{\circ}$C so that water vapour with a desired concentration was generated. The carrier gas (N_2) with a flow rate of 400 ml/min was purged through a mercury permeation device placed in a sealed U-shaped quartz tube to introduce a continuous feed of Hg^0 (about 90 ± 0.2 $\mu g/m^3$) to the reaction system. The relatively high Hg^0 concentration in comparison to that of the real flue gas of a coal-fired boiler was used to avoid/minimize experimental errors. The adsorption tests were carried out by using 200 mg prepared sorbents locating in a quartz glass tube reactor with an inner diameter of 8 mm and length of 80 mm. The glass tube reactor was placed in a temperature controlled tubular furnace to realize an intended reaction temperature with fluctuations less than 2 $^{\circ}$C. The sorbents was grinded into 40 - 60 meshes particles (i.e. 250 - 425 μm), and the gas hourly space velocity (GHSV) was controlled to be about 4×10^5 h^{-1}. The Hg^0 removal performance of each selected sorbent under various flue gas compositions atmosphere was determined at 150 $^{\circ}$C which more or less reflected the real flue gas temperature of coal-fired boilers [40]. The Hg^0 concentration of the outlet gas was detected by an online continuous vapour-mercury analyzer with the accuracy of 0.1 ug/m^3 and the detection limit of 0.1 ug/m^3 (VM3000, Mercury Instruments, Germany). The exhaust gas containing uncaptured Hg^0 and other gas components was passed through a NaOH solution and an activated carbon filter before discharge. The simulated flue gas was diverted to the bypass line for the determination of the baseline of primary inlet Hg^0 concentration before each test.

The Hg^0 removal efficiency η was calculated according to the following equation:

$$\eta = (1 - C_{out}/C_{in}) \tag{1}$$

where C_{in} and C_{out} represented Hg^0 concentrations of the inlet and outlet of the fixed-bed reactor, respectively.
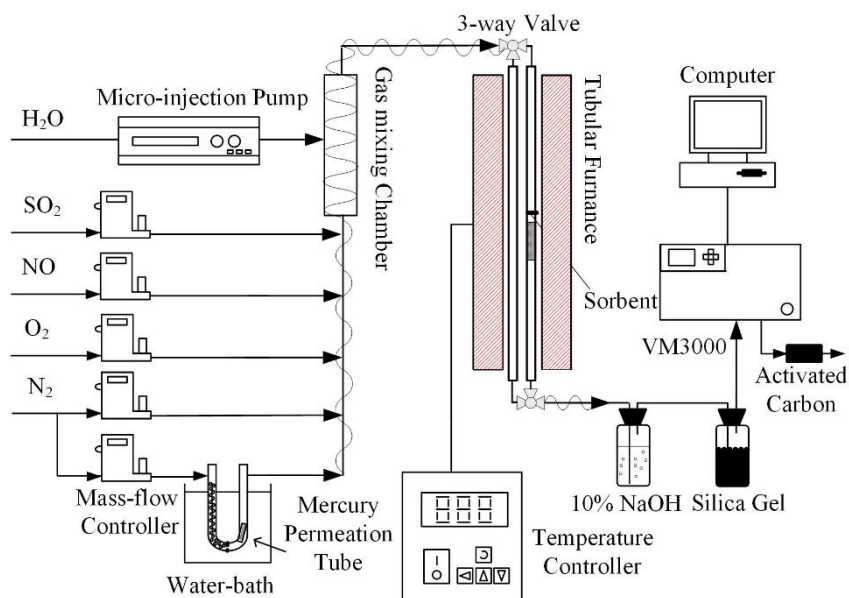
Fig. 2 Experimental schematic diagram of mercury adsorption fixed bed system.

3 Results and discussion

3.1 Sample characterization

The crystal phase of ATT and xFe1ATT samples was determined by XRD analysis (Fig. 3). The typical diffraction peaks at 2θ values of 13.7°, 19.9°, 26.7°, and 35.3° correspond to the primary diffraction of the (2 0 0), (0 4 0), (4 0 0), and (1 6 1) planes of ATT (JCPDS No. 00-021-0550), respectively, indicating the high layer chain structure of ATT [38, 41-43]. After the introduction of γ-Fe$_2$O$_3$ into ATT, the characteristic peaks of ATT became weak apparently. The peaks at 2θ = 30.3°, 35.7°, 57.4°, and 62.9°

10

can be ascribed to the planes (2 2 0), (3 1 1), (5 1 1) and (4 0 0) of γ-Fe_2O_3, according to the JCPD standards of γ-Fe_2O_3 (JCPDS No. 39-1346) [35, 44]. The intensity of the γ-Fe_2O_3 peaks strengthened gradually with an increase in the γ-Fe_2O_3 loading amount. These results imply that the magnetic xFe1ATT composites had been successfully synthesized.
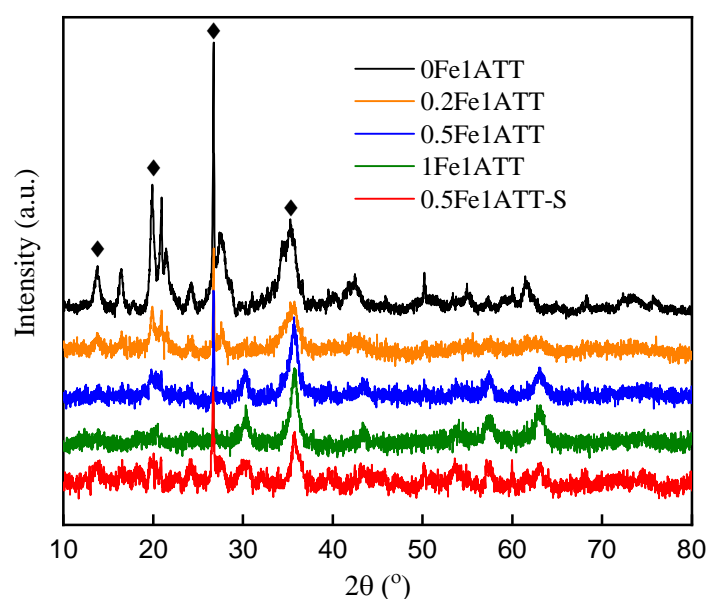

Fig. 3 XRD patterns of pure ATT and xFe1ATT samples.

The TEM analysis was performed to study the surface textures and morphologies of the prepared sorbents. As shown in Fig. 4 (a), the typical TEM image of ATT reveals that ATT contains a smooth rod-like morphology with an average diameter of 20-40 nm and a length of 400-800 nm. Such fiber structure favours the loading of the metal oxide particles on its surface [39]. After the introduction of γ-Fe_2O_3 (Fig. 4 (b-d)), small particles appear on the surface of ATT with the diameter of 3-10 nm, indicating the successful loading of iron oxide. More particles appeared on the surface of ATT and

11

the aggregation of the particle could also be observed at the same time with the increasing loading of γ-Fe_2O_3 as shown in Fig. 4 (c) and (d). A serious aggregation of particles could be observed for 1Fe1ATT with the highest loading amount of γ-Fe_2O_3 as shown in Fig. 4 (d), which is detrimental to the dispersion of the active substance and, hence, impairing the Hg^0 adsorption ability.
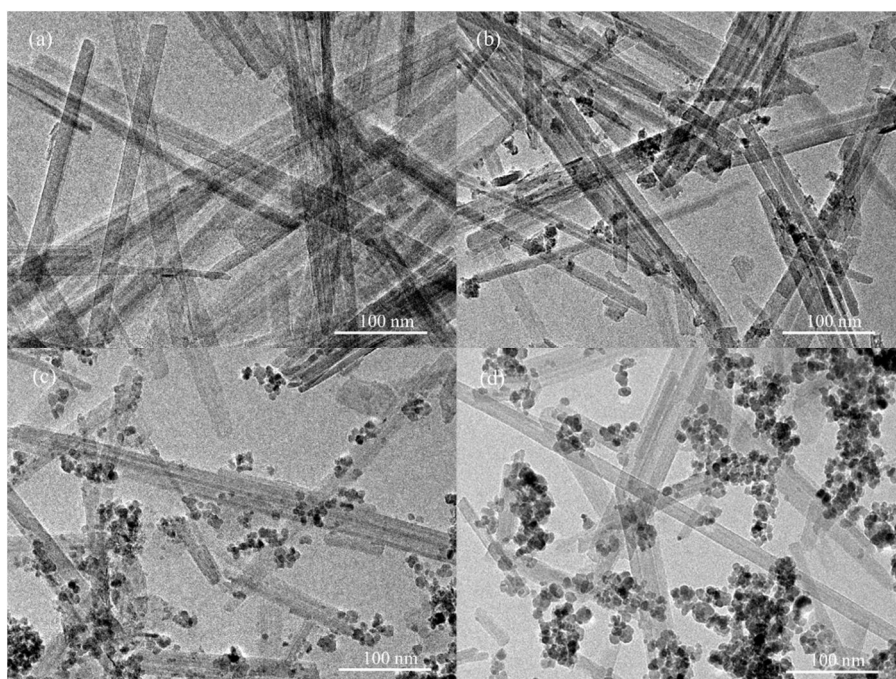

Fig. 4 TEM images of pure ATT (a), 0.2Fe1ATT (b), 0.5Fe1ATT (c), and 1Fe1ATT (d) samples.

The nitrogen adsorption-desorption isotherms of xFe1ATT samples are shown in Fig. 5. It can be seen that the isotherm profiles of all samples display a type II adsorption isotherm, according to the IUPAC classification, which indicates that all samples are of the mesoporous structure [35]. The SSA, total pore volume and average pore size

properties of the samples (γ-Fe_2O_3, xFe1ATT) are shown in Fig. 6. It can be observed that the BET surface area of the samples follows a descending order: 0Fe1ATT > 0.2Fe1ATT > 0.5Fe1ATT > 1Fe1ATT > γ-Fe_2O_3. The raw ATT possessed the largest SSA and the largest pore volume, resulting in its large adsorption capacity. When γ-Fe_2O_3 was loaded onto ATT, both the BET surface area and pore volume of the modified samples decrease gradually. The average pore diameter was decreased initially after the introduction γ-Fe_2O_3 of into ATT, but then increased with the increase of γ-Fe_2O_3 loading mount. This might be ascribed to the newly formed macropores on the surface of ATT due to the excessive loading of γ-Fe_2O_3, and the blocking of the inner pores of ATT. The pure γ-Fe_2O_3 had the lowest surface area indicating a small area contacting with gaseous mercury, which might go against the adsorption and oxidation reaction of gas-solid reaction.
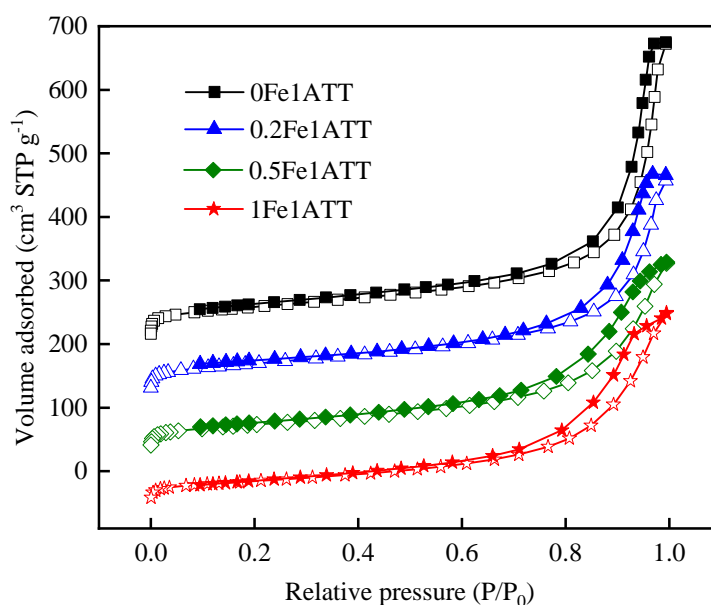

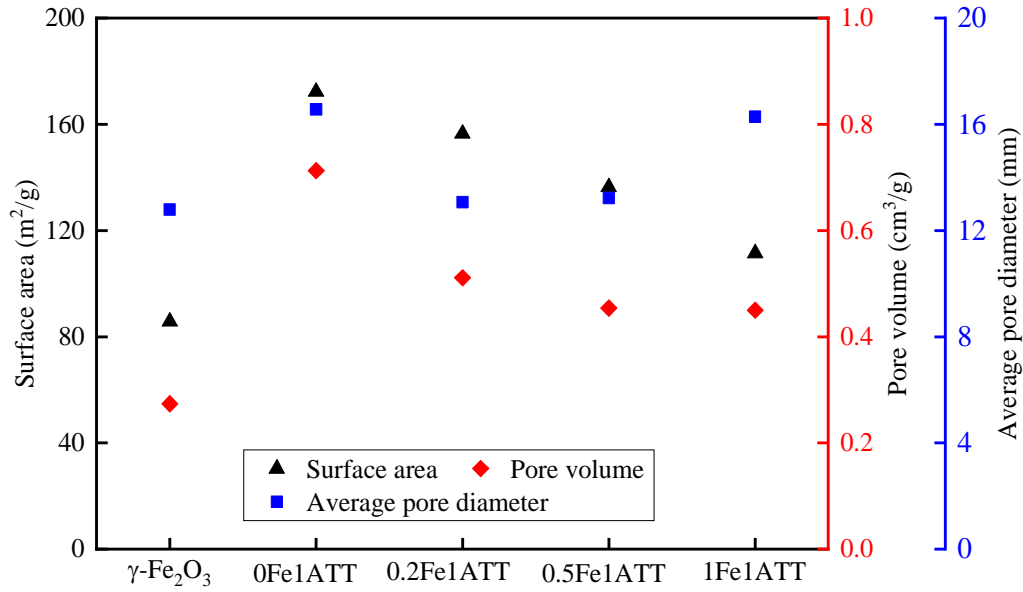**Fig. 5** N_2 adsorption–desorption isotherms obtained at 77 K of xFe1ATT samples.

Fig. 6 Specific surface area and pore structure of the pure γ-Fe$_2$O$_3$ and xFe1ATT samples.

A key feature of the prepared sorbents is the magnetic characteristic, which makes it capable to be separated from the fly ash and then captured by the PCD. The magnetic hysteresis curves of the γ-Fe$_2$O$_3$ modified attapulgite composites are shown in Fig. 7. Negligible coercivity and magnetization hysteresis of the samples were observed, indicating the successful synthesized of superparamagnetic sorbents. The saturation magnetizations of the γ-Fe$_2$O$_3$ and xFe1ATT (x=0.2, 0.5, 1) were 45.1, 29.5, 18.0, and 5.2 emu/g, respectively. The insert photograph in Fig. 7 demonstrates that the prepared 0.5Fe1ATT samples could be separated from the mixture of 2.0 g of sand and 0.2 g of 0.5Fe1ATT sorbents by an external magnet.
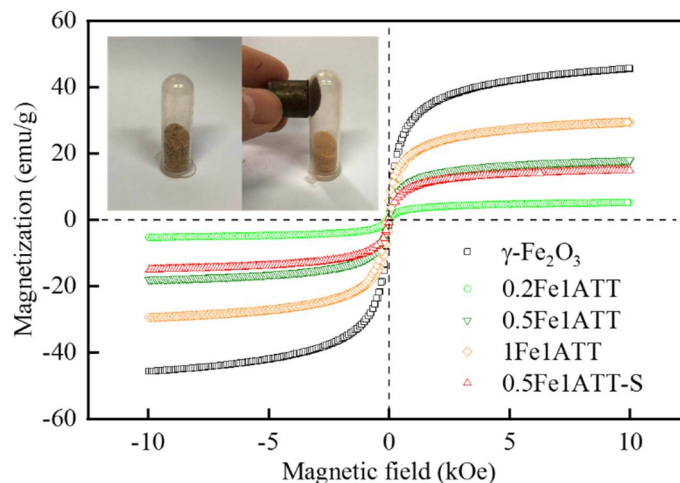
Fig. 7 Magnetization characteristics of γ-Fe_2O_3，xFe1ATT and SO_2 reacted samples.

The XPS spectra were obtained for the O 1s, Fe 2p, and Si 2p regions to characterize the surface elements valence state of the fresh sorbent, as shown in Fig. 8. Four peaks at about 530.2 eV, 532.1 eV, 533.1 eV and 534.3 eV were observed on the 0.5Fe1ATT (Fig. 8 (a)), which can be attributed to lattice oxygen in metal oxides (O_L) [37], chemisorbed oxygen (O^*) [45], lattice oxygen in silicon oxides (O_s) [46] and oxygen exists in chemisorbed water (O_w) [47], respectively . As shown in Fig. 8 (b), the two main peaks appeared at 711.6 eV and 725.3 eV which can be ascribed to the Fe $2p_{3/2}$ and Fe $2p_{1/2}$ spectra, respectively [35]. The peak at around 718.3 eV can be seen clearly, verifying the presence of γ-Fe_2O_3 in sorbent, which is consistent with the previous reports [35, 48]. Besides, the spectra of Fe $2p_{3/2}$ can be fitted into three characteristic peaks [16]: the peak centered at about 710.2 eV which is assigned to the Fe^{2+} ion and the peaks center at 711.5 eV and 713.8 eV which can be attributed to Fe^{3+} in octahedral

15

coordination and Fe^{3+} in tetrahedral coordination, respectively [49]. As shown in Fig. 8

(d), the peak at about 103.1 eV over the fresh sorbent can be ascribed to Si 2p [16].
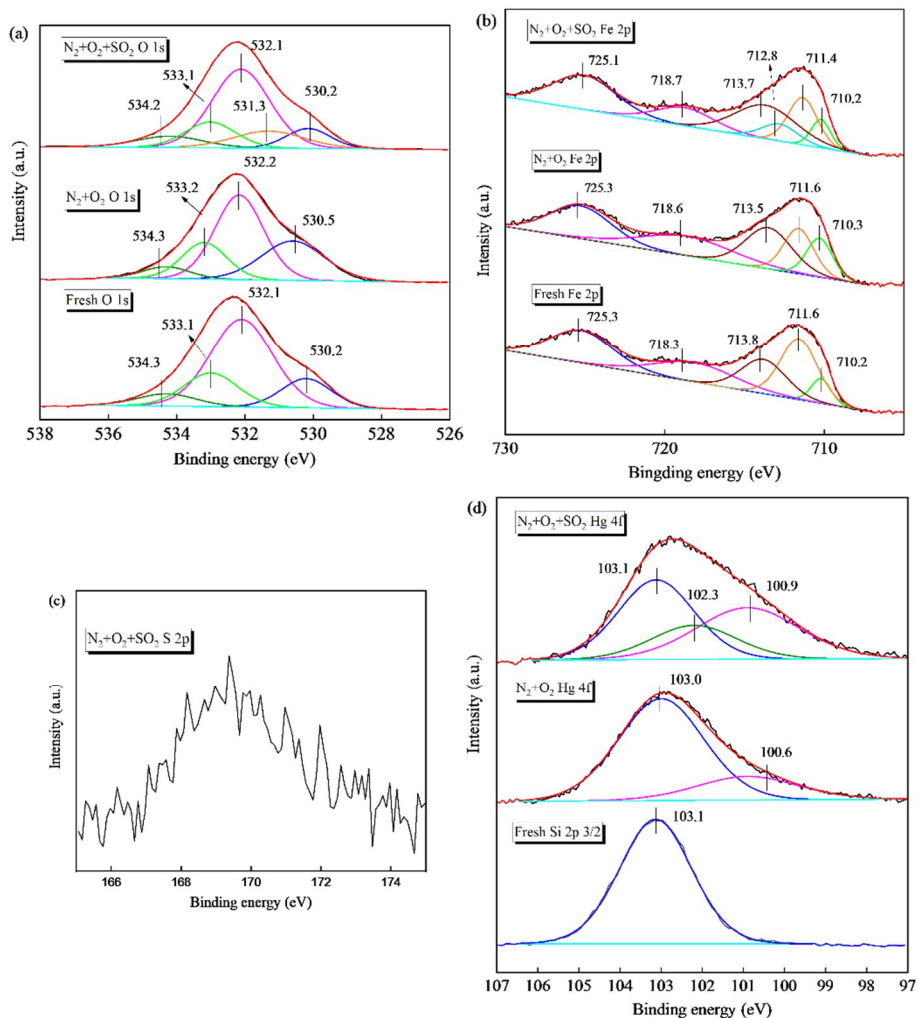

Fig. 8 XPS spectra of O 1s (a), Fe 2p (b), S 2p (c), and Hg 2p (d) over fresh and spent 0.5Fe1ATT samples.

In order to investigate the surface groups of the 0.5Fe1ATT sample, FTIR analysis

was performed as shown in Fig. 9. The peaks at around 483 and 1050 cm^{-1} are attributed

to the Si-O-Si bonds [38]. The peaks at about 1610 and 3490 cm^{-1} can be assigned to the

bend vibration of zeolite water [38]. The band at about 630 cm^{-1} can be ascribed to Fe-O

16

stretching modes of tetrahedral and octahedral sites in the inverse spinel structure of γ-Fe_2O_3 [50]. The results of FTIR analyses indicate that the successful corporation of γ-Fe_2O_3 into attapulgite was achieved in this work.
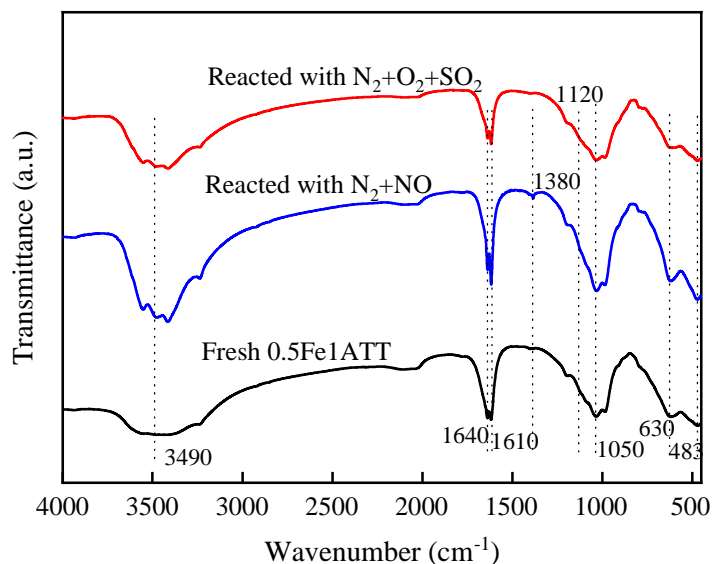

Fig. 9 FTIR spectra of the fresh, NO and SO_2 reacted 0.5Fe1ATT samples.

3.2 Mercury adsorption efficiency of different samples

Hg^0 removal efficiencies over the γ-Fe_2O_3 modified attapulgite with different γ-Fe_2O_3/attapulgite mass ratios under an atmosphere of 5% O_2, 12% CO_2 and N_2 (balance) at 150 $^\circ$C are shown in Fig. 10. No apparent Hg^0 removal was observed over pure ATT, and the removal efficiency, η, in the entire period of experiment time was less than 10%. The result was in line with an earlier study in which about 20% of Hg^0 introduced was removed over ATT [36]. The poorer Hg^0 removal performance in this study was ascribed to the higher GHSV and higher Hg^0 inlet concentration. The addition of Fe_2O_3 resulted in significant enhancement of Hg^0 removal activity, about

17

30% of Hg^0 removed over 0.2Fe1ATT at the end of the test time at 150 ^oC. Since pure ATT was essentially inactive for the removal of Hg^0, Hg^0 removal performance observed was attributed to the activity of γ-Fe_2O_3 supported on ATT. The introduction of Fe_2O_3 creates a series of active sites that favour the interaction between Hg^0 and the composites. Since Fe_2O_3 was the active component of the xFe1ATT sorbents that was really effective in the Hg^0 removal reaction, the loading amount of Fe_2O_3 was expected to be a decisive factor for Hg^0 adsorption. Hence, a higher loading amount of Fe_2O_3 should result in more active sites for elevating the chemisorption of mercury. As it can be observed in Fig. 10, the Hg^0 removal performance of the sorbents was elevated with the increase in the loading amount of Fe_2O_3. However, it can also be noticed that the Hg^0 removal efficiency of pure Fe_2O_3 sorbent was only higher than that of 0.2Fe1ATT but lower than that of the other γ-Fe_2O_3 loaded ATT sorbents. This can be explained by the fact that the gas mercury removal process by the solid sorbent is a gas-solid reaction, and hence is affected by the contact surface. Although the pure Fe_2O_3 sorbent had the highest amount of active Fe_2O_3, its BET surface and the pore volume were very low, hence it could not supply enough active sites on the sorbent surface. The Fe_2O_3 loading amount of 1Fe1ATT was doubled as compared with that of 0.5Fe1ATT. However, the mercury removal efficiency was only increased from 75% of 0.5Fe1ATT to 81% of 1Fe1ATT with an increment of 6%. This observation was likely due to the decrease of the SSA that was confirmed by the BET analysis, which resulted in poorer physisorption of Hg^0 over the sorbents [24]. As depicted in Fig. 7, the 1Fe1ATT and

0.5Fe1ATT both had a moderate saturation magnetization and could be easily separated from the fly ash from our tests. However, the 0.5Fe1ATT sample used only half the amount of Fe_2O_3 as the 1Fe1ATT sample, indicating a much lower cost to achieve the comparative mercury control performance, which should be an important consideration in practical applications. Therefore, the optimal loading amount of γ-Fe_2O_3 for mercury capture was considered to be at the mass ratio of Fe/ATT = 1:2 (0.5Fe1ATT), and was selected as the default loading amount in the subsequent experiments.
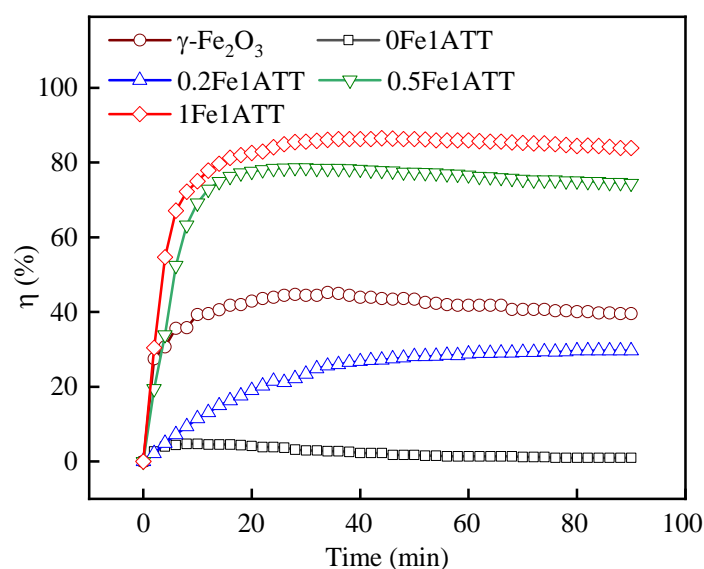

Fig. 10 Effect of γ-Fe_2O_3/attapulgite mass ratios on Hg^0 removal performance (150 ^{o}C, N_2+5% O_2).

3.3 Effect of adsorption temperature

The temperature of the coal-fired boiler flue gases before the particulate control device is generally less than 250 ^{o}C and higher than 100 ^{o}C. Therefore, the adsorption temperature range of 100-250 ^{o}C was selected to investigate its effects on Hg^0 removal performance over 0.5Fe1ATT, which were also studied by other researchers [51, 52]. As

19

shown in Fig. 11, it can be seen that the Hg^0 removal efficiency within 90 min increased from 34.4% to 83.1% with the temperature rising from 100 $^\circ$C to 250 $^\circ$C. The increasing trend was similar to the results of Fe_2O_3-SiO_2 sorbent [24]. But the Hg^0 removal efficiency of 0.5Fe1ATT was higher than that of Fe_2O_3-SiO_2 sorbent although the GHSV in this study was much higher. The reason was that the introduction of Fe_2O_3 into ATT enhanced the iron oxide dispersion on the surface, which was in favour of the adsorption reaction with the active sites. The mercury removal efficiency significantly increased from 34.4% to 75.3% with the temperature rising from 100 $^\circ$C to 150 $^\circ$C. A higher temperature benefits the chemisorption for mercury removal while a lower temperature contributes to the physisorption. As is well-known, chemisorption is more favourable than physisorption for mercury removal by metal oxide sorbents. Further increasing the reaction temperature to 200 $^\circ$C and 250 $^\circ$C resulted in small increments of mercury removal efficiency, at 5.3% and 7.5%, respectively. It is generally recognized that the gas Hg^0 is firstly adsorbed on the sorbent surface to form the adsorbed Hg^0 species and subsequently is oxidized and chemisorbed during the Hg^0 removal process [37]. An increase in the reaction temperature could inhibit the adsorption of Hg^0, and hence the subsequent chemisorption was inhibited accordingly [16]. Besides, the release of chemisorbed mercuric species on the surface of sorbents might occur at high temperatures [24]. Hence, the adverse effect of temperature increase could offset the limited enhancement of chemisorption of Hg^0.
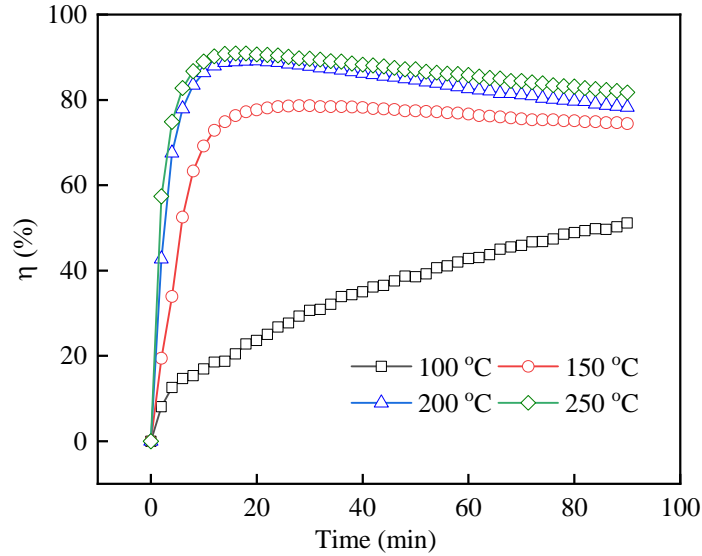
20

Fig. 11 Effect of reaction temperature on Hg^0 removal performance 0.5Fe1ATT sample (N_2+5% O_2).

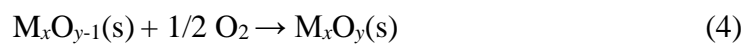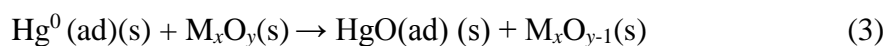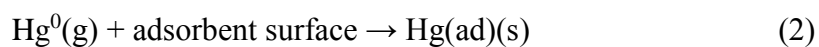## 3.4 Effects of individual flue gas components

The effects of individual flue gas components were investigated to understand the role of each component in the coal-fired boiler flue gases for Hg^0 removal.

3.4.1 Effect of O_2

O_2 was one of the main gas components in flue gas and could have a critical role in the mercury adsorption reaction. To understand the effect of O_2 concentration on mercury removal, Hg^0 removal with 0.5Fe1ATT was conducted with flue gases containing various concentrations of oxygen at 150 ^{o}C and the results are shown in Fig. 12. It can be found that a significant increase in Hg^0 removal efficiency appeared when 5% O_2 was added to the flue gas without O_2. Gas-phase O_2 in flue gas could replenish and regenerate the consumed surface oxygen on the adsorbent surface [53], which served

as the oxidants consumed during Hg^0 oxidation process. As shown in Fig. 8 (a) and

Table 1, after the Hg^0 adsorption experiments under N_2 and 5% O_2, the content of O_L

increased from 15.4% to 28.2%, while the content of O* decreased from 57.9% to

46.9%. These results suggest that O* participated in the Hg^0 oxidation reaction. The

increase of O_L in the spent 0.5Fe1ATT sorbent compared to that in the fresh sorbent

could be ascribed to the appearance of O^{2-} in HgO [37]. Table 1 also shows that the content

of Fe^{2+} increased from 6.9% to 12.5% after Hg^0 adsorption, which can be ascribed to

the reduction of Fe^{3+} during the Hg^0 oxidation process. For the spectra of Hg 4f over

spent 0.5Fe1ATT as shown in Fig. 8 (d), the peak at about 103.1 eV corresponding to

Si 2p can be observed, and the other new peak at about 100.6 eV has appeared that can

be assigned to the Hg^{2+} in HgO [54], indicating the oxidization of Hg^0 has occurred during

its adsorption process over 0.5Fe1ATT. Meanwhile, the TPD analyses of the Hg^0

adsorption over 0.5Fe1ATT in the absence and presence of 5% O_2 were carried out as

shown in Fig. 13. For the Hg^0 adsorption under N_2, one Hg desorption peak observed

at around 315 °C can be attributed to HgO [55]. Compared with the adsorption of N_2 +

Hg^0, the mercury desorption peak moves to a higher temperature at 345 °C and the

desorption peak area becomes much larger, during the adsorption in the presence of 5%

O_2. This indicates that O_2 could greatly promote Hg^0 adsorption. From above, the Hg^0

removal in the presence of O_2 can be explained as the Mars-Maessen mechanism [19],

which is described by reactions (2)-(5) [24]. The adsorbed elementary mercury can react

22

with the surface oxygen existed on the surface of metal oxides (M_xO_y). The M_xO_y in

this study is Fe_2O_3, while the intermediate product can be Fe_3O_4 or FeO.

$$Hg^0(g) + \text{adsorbent surface} \rightarrow Hg(ad)(s) \qquad (2)$$

$$Hg^0(ad)(s) + M_xO_y(s) \rightarrow HgO(ad)(s) + M_xO_{y-1}(s) \qquad (3)$$

$$M_xO_{y-1}(s) + 1/2\ O_2 \rightarrow M_xO_y(s) \qquad (4)$$

$$HgO(ad)(s) + M_xO_y(s) \rightarrow HgM_xO_{y+1}(s) \qquad (5)$$

As the oxygen concentration was further increased to 10% from 5%, the mercury

efficiency showed negligible increase and stayed at approximately 78% (Fig. 12). This

observation indicates that 5% O_2 was enough for regenerating and replenishing the

oxidants and a higher oxygen concentration would not result in a further improvement
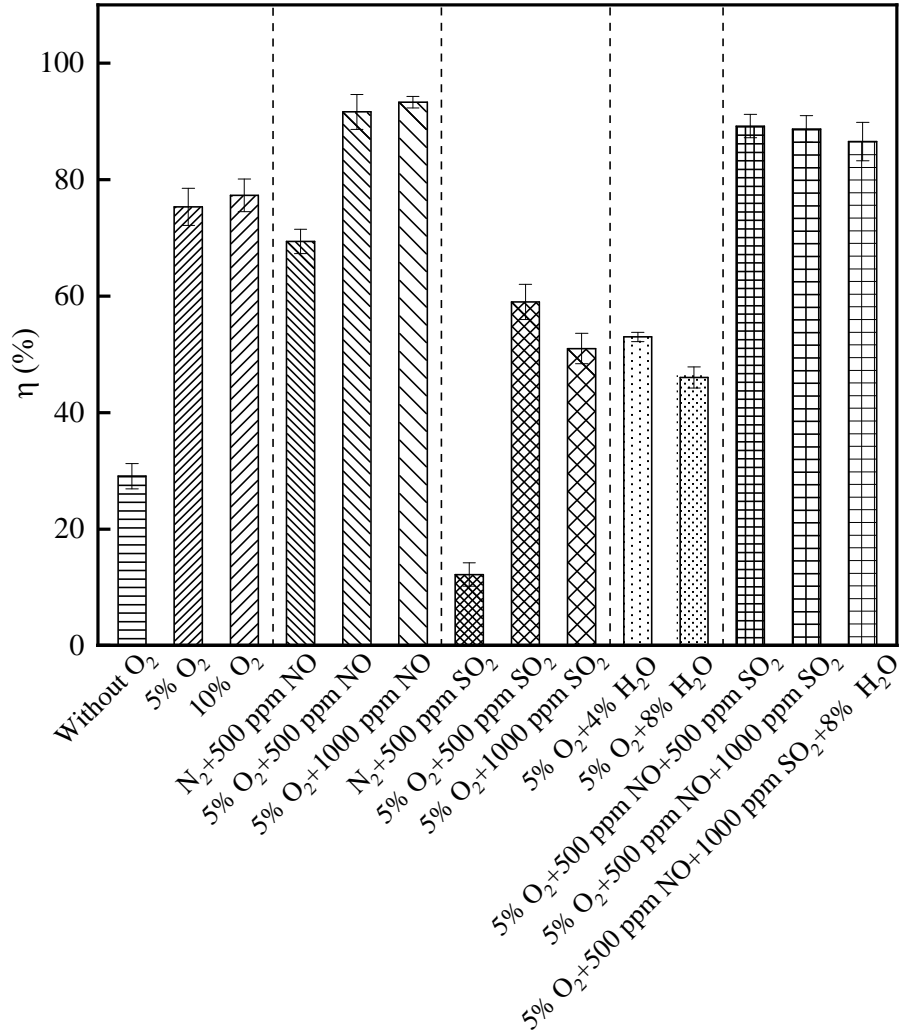
of the mercury removal performance [45].

Fig. 12 Effect of flue gas components on Hg^0 removal performance over 0.5Fe1ATT sample (150 °C, N_2 as the balance).

Table 1 Molar concentration of surface atoms on the catalysts (detected by XPS).

Sample	O 1s (%)		Fe 2p (%)
	O_L/O	O^*/O	Fe^{2+}/Fe
Fresh	15.4	57.9	6.2
Reacted with N_2+O_2	28.2	46.9	12.5
Reacted with $N_2+O_2+SO_2$	10.1	52.4	6.9
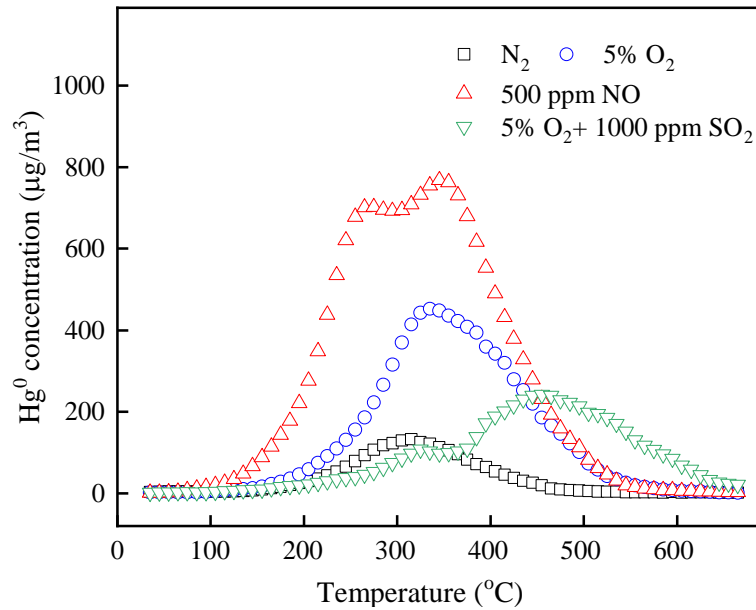
Fig. 13 Hg-TPD curves under different adsorption conditions (adsorption at 150 $^{\circ}$C).

3.4.2 Effect of NO

Normally the coal-fired boiler flue gases will contain a small amount of NO even with the most advanced NO_x emission control strategies such as SCR being adopted by the plant. Hence, the interaction between NO and Hg^0 should be taken into consideration to figure o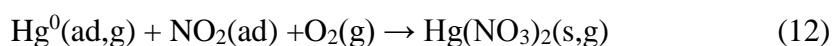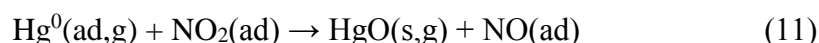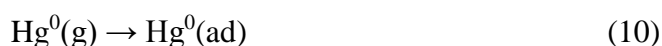ut the effect of NO on the mercury removal of the 0.5Fe1ATT sorbent. The results on mercury removal efficiency of 0.5Fe1ATT under different NO concentrations are shown in Fig. 12. It can be seen that an addition of 500 ppm NO to N_2 resulted in a significant enhancement to the Hg^0 removal, reaching 69.4% Hg^0 removal efficiency, which was much higher than that achieved with the pure N_2 atmosphere (28.0%). With the further assistance of O_2, the Hg^0 removal efficiency increased substantially and reached 91.6%. This observation could be ascribed to the

formation of NO^+ or NO_2 due to the adsorbed NO oxidized on the surface of metal

oxide sorbents [56, 57]. The influence of NO on mercury adsorption could be interpreted

by the following reactions (5-13):

$$NO(g) + \text{adsorbent surface} \rightarrow NO(ad) \tag{5}$$

$$NO(ad) + M_xO_y(s) \rightarrow NO\text{-}O\text{-}M_xO_{y\text{-}1}(s) \tag{6}$$

$$NO\text{-}O\text{-}M_xO_{y\text{-}1}(s) \rightarrow NO_2 + M_xO_{y\text{-}1}(s) \tag{7}$$

$$O_2(g) \rightarrow O_2(ad) \tag{8}$$

$$NO(ad) + O_2(ad) \rightarrow NO_2(ad) + O \tag{9}$$

$$Hg^0(g) \rightarrow Hg^0(ad) \tag{10}$$

$$Hg^0(ad,g) + NO_2(ad) \rightarrow HgO(s,g) + NO(ad) \tag{11}$$

$$Hg^0(ad,g) + NO_2(ad) + O_2(g) \rightarrow Hg(NO_3)_2(s,g) \tag{12}$$

$$HgO(ad,g) + 2NO(ad) + 3/2O_2(g) \rightarrow Hg(NO_3)_2(s,g) \tag{13}$$
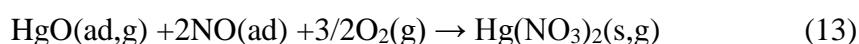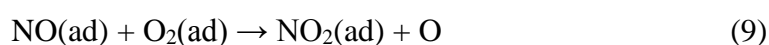
Under the pure N_2 atmosphere, NO was weakly adsorbed on the metal oxide and

subsequently be oxidized by lattice oxygen and/or chemisorbed oxygen on the surface

to form limited new species, such as NO^+, NO_2, and NO_3^- [19]. Then adsorbed Hg^0 could

interact with NO_2 to form HgO and $Hg(NO_3)_2$ via reactions (5-7) and (10-13). However,

the surface oxygen on the sorbent, which played a crucial part in mercury adsorption,

was consumed via the above reactions (6) and (7), hence, lack of O_2 in the flue gas

inhibited Hg^0 removal. In the presence of O_2, more adsorbed NO could be oxidized on

the sorbent to form abundant active species like NO_2 via reactions (8) and (9).

Furthermore, the gas phase O_2 could regenerate and replenish the consumed surface

oxygen via reaction (4). Both of the above two reasons contribute to the enhanced

mercury removal as a result of the addition of NO in the presence of O_2 atmosphere.

From the FTIR curve of the 0.5Fe1ATT sorbent which reacted in the atmosphere of N_2+500 ppm NO as depicted in Fig. 9, the peaks at 1380 cm^{-1} and 1640 cm^{-1} can be assigned to the nitrate species and adsorbed NO_2 [11]. The existence of these two bands indicated that 0.5Fe1ATT could oxidize NO into NO_2 without the presence of O_2, hence, promoting the Hg^0 oxidation. In order to analysis the mercury species existed on the surface of the 0.5Fe1ATT sample after Hg^0 adsorption under N_2+500 ppm NO, the TPD was performed as shown in Fig. 13. Two desorption peaks observed at about 280 ^oC and 355 ^oC can be ascribed to $Hg(NO_3)_2$ [58] and HgO , respectively. The peak area is much larger than that of the Hg^0 adsorption under O_2 atmosphere, indicating an improved Hg^0 adsorption ability can be realized with the help of NO. In addition, the introduction of O_2 would accumulate more NO_2 and nitrate species on the surface of the sorbent, which could further promote the Hg^0 oxidation. However, a further increase in NO concentration to 1000 ppm only led to a slight promotional effect on mercury removal (Fig. 12) and this could be the fact that the non-active species like nitrate might be generated and then covered the active adsorption/oxidation sites [19, 57].

3.4.3 Effect of SO$_2$

SO$_2$ is another gaseous pollutant presents in coal-fired boiler flue gases. The effect of SO$_2$ on Hg^0 adsorption by metal oxides is still not conclusive. Detrimental [59], negligible [56], promotional [24], and bifacial [60] effects of SO$_2$ on Hg^0 adsorption have all been observed by previous investigations. In the present study, a detrimental influence

of SO_2 on Hg^0 adsorption over the 0.5Fe1ATT sorbent was found both in the absence

and presence of O_2 as shown in Fig. 12. The addition of 500 ppm SO_2 to the pure N_2

atmosphere resulted in a significant decrease in the Hg^0 removal efficiency, η, from

28% to 12.2%. According to the previous studies [37, 61], SO_2 could inhibit Hg^0 oxidation

via the following three routes: (1) The reaction between SO_2 and the oxygen species on

the surface of sorbent; (2) The competitive adsorption between SO_2 and Hg^0 for the

same active sites on the sorbent surface; (3) The sulfation of metal oxide under the

atmosphere of SO_2. Without the presence of O_2 in the reaction environment, SO_2

inhibited Hg^0 oxidation over 0.5Fe1ATT sorbent by consuming the surface oxygen

species and hence significantly suppressed Hg^0 removal. Also shown in Fig. 12, the

presence of 5% O_2 in the reaction gas environment obviously alleviated the suppressive

effect of SO_2, indicating the inhibitive effect of SO_2 was largely attributed to the route

(1) as the surface oxygen of the sorbent consumed by SO_2 could be replenished and

regenerated after the introduction of O_2. However, the Hg^0 removal efficiency

decreased from about 60% to 51% when the added SO_2 concentration to the reaction

environment containing 5% O_2 was increased from 500 ppm to 1000 ppm. This

indicates route (1) could only partially account for the deactivation of 0.5Fe1ATT in

the presence of O_2. To understand the inhibition effect of route (2), additional

experiments were carried out in the present study. The competitive adsorption between

SO_2 and Hg^0 could be verified by a desorption experiment [19]. The 0.5Fe1ATT sorbent

was first exposed to Hg^0 plus pure N_2 at 150 ^{o}C for 90 min. Then Hg^0 was cut off and

28

1000 ppm SO_2 was introduced into the flue gas. From the results in Fig. 14, the concentration of Hg^0 was suddenly increased from nearly zero to 43 ug/m^3 after simultaneously cutting off Hg^0 and adding SO_2. This suggests that introducing SO_2 into the reaction system resulted in the desorption of the weakly bounded mercury on the sorbent surface from the surface of the sorbent. That is to say, the competitive adsorption of SO_2 and Hg^0 was occurring during the Hg^0 removal process over the 0.5Fe1ATT sorbent [57]. Further experiments were also carried out to check the relevance of route (3), i.e. to check if SO_2 had reacted with iron oxide on the sorbent forming metal sulfate. These experiments on the Hg^0 removal activity were performed with the SO_2 pretreated sorbent. The sorbent was first pretreated with 500 ppm SO_2 under 5% O_2 atmosphere at 150 ^{o}C for 1 h and 3 h before Hg^0 adsorption tests to eliminate the impact of the competitive adsorption between SO_2 and Hg^0. As shown in Fig. 15, the Hg^0 removal ability of the sorbent was significantly impaired after being pretreated by SO_2. The results confirm the relevance of route (3) to the sorbent of this study, i.e. that the introduced SO_2 had reacted with the metal oxide to form some sulfate species that were inert for Hg^0 removal [19]. It was reported that SO_2 has a promotional effect on elemental mercury oxidation over α-Fe_2O_3 with the aid of O_2 at 300 ^{o}C [24], contradicting to the observation of this study which investigated mercury oxidation at a much lower temperature of 150 ^{o}C. This is mainly due to the fact that the higher temperature weakens the SO_2 adsorption over the sorbent surface [62]; the oxidation of SO_2 to SO_3 could also result in new chemisorption sites that benefit elemental mercury removal at

29

a higher temperature [24]. In order to investigate the sulfation of 0.5Fe1ATT sorbent had occurred, the XRD analysis of the sorbent that reacted under the environment of N_2+5% O_2+1000 ppm SO_2 (donated as 0.5Fe1ATT-S) was performed as shown in Fig. 3. Compared with the fresh sorbent, no clearly new peaks can be observed in 0.5Fe1ATT-S, which can be ascribed the fact that the formed sulfate species are too low in quantity to be detected by XRD or might exist as amorphous sulfate [59]. Hence, further characterization of the spent sorbent by the means of XPS and FTIR analysis was performed to testify the sulfation. As shown in Fig. 8 (a) and (b), after Hg^0 adsorption, the XPS spectras of O 1s and Fe 2p of the 0.5Fe1ATT-S show a new fitting peak at about 531.3 eV and 712.9 eV, which could be ascribed to the species of SO_4^{2-} and $Fe_2(SO_4)_3$, respectively [45]. Besides, SO_4^{2-} was also detected on the S 2p spectra of the SO_2 reaction sorbent as shown in Fig. 8 (c) [59]. This suggests that SO_2 has reacted with the sorbent to form sulfate species, which is inert for Hg^0 adsorption. The FTIR analysis of the 0.5Fe1ATT-S was also performed in order to investigate the form of the surface sulfur species as shown in Fig. 9. The bands at 1050 cm^{-1} and 1120 cm^{-1} can be ascribed to the ν(S=O) vibration of sulfate species or molecularly chemisorbed SO_2 [59]. Hence, the FITR analysis also verified the surface sulfation after the reaction with SO_2. For the spectra of Hg 4f as shown in Fig. 8 (d), the newly formed peaks of the SO_2 reacted sorbent appeared at about 100.9 eV and 102.3 eV correspond to the Hg^{2+} species from HgO and $HgSO_4$, respectively [59, 63]. In order to further verify the existence of $HgSO_4$ on the surface of the 0.5Fe1ATT-S, the TPD analysis was used and the desorption curve

is shown in Fig. 13. It can be seen that the desorption peak of mercury ranges from 380 $^{\circ}$C to 650 $^{\circ}$C, peaking at about 475 $^{\circ}$C, corresponding to the decomposition of $HgSO_4$ [58], hence, evidencing the existence of $HgSO_4$ on the surface of the used sorbent after the reaction with SO_2. Meanwhile, a small shoulder peak at 330 $^{\circ}$C is also observed that can be assigned to HgO. Although the sulfation of the 0.5Fe1ATT sorbent occurred after the reaction with SO_2, the saturation magnetization of 0.5Fe1ATT-S was only reduced slightly comparing to that of the fresh sample and still remained at 14.9 emu/g as shown in Fig. 7. Negligible coercivity and magnetization hysteresis of 0.5Fe1ATT-S were also observed from Fig. 7, indicating the superparamagnetic maintained after being treated with SO_2.

Interestingly, the inhibition of SO_2 on Hg^0 removal activity over 0.5Fe1ATT sorbent could be greatly alleviated by the introduction of NO, as observed in Fig. 12. The mercury removal efficiencies of 0.5Fe1ATT in the presence of 500 ppm SO_2 and 1000 ppm SO_2 both reached about 88% with the addition of 500 ppm NO, which was significantly higher than that was achieved with the flue gases containing SO_2 without NO. This phenomenon might be ascribed to the different adsorption active sites on the surface of sorbent between SO_2 and NO. NO and SO_2 always co-exist in actual coal-fired boiler flue gases and hence the inhibitory effect of SO_2 on the Hg^0 removal by the sorbent can be somewhat offset by the presence of NO in the flue gas.
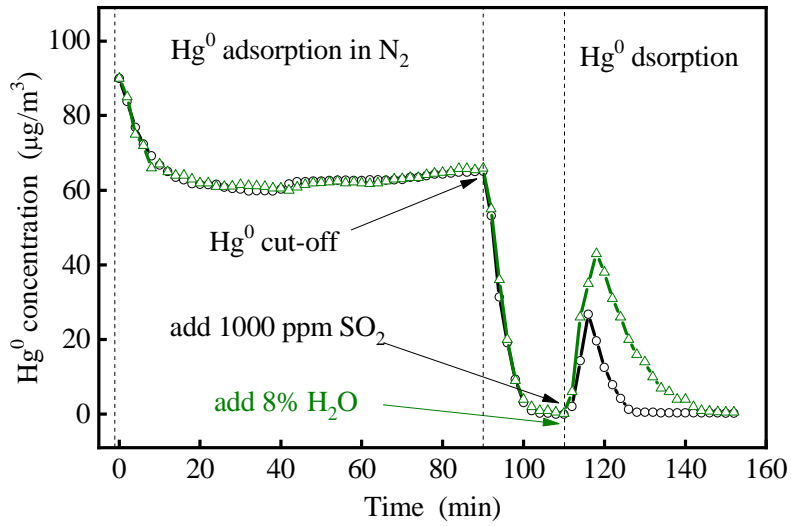
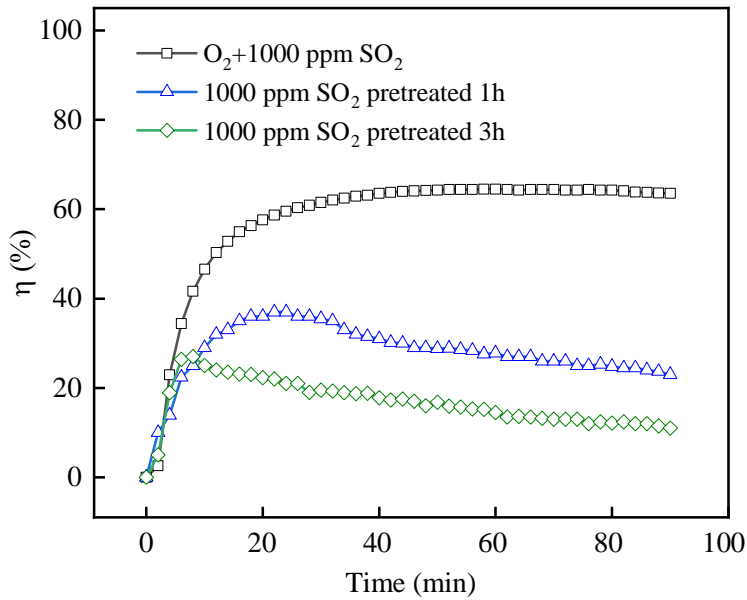**Fig. 14** Hg^0 desorption by SO_2 or H_2O over 0.5Fe1ATT sample at 150 °C.

Fig. 15 Hg^0 removal performance over SO_2 pretreated 0.5Fe1ATT sample (150 °C, N_2 as the balance).

3.4.4 Effect of H_2O

Water vapour is one of the main components in coal-fired boiler flue gases and can adversely affect the Hg^0 removal performance over metal oxide based sorbents [19, 57]. As

shown in Fig. 12, H_2O significantly impaired Hg^0 removal performance over 0.5Fe1ATT sorbent. A decrement of 13% for the Hg^0 removal efficiency was observed when 4% H_2O was added into the reaction flue gas. A further increase in the added H_2O to 8% reduced the Hg^0 removal efficiency to 51%. It has been reported that the inhibition of H_2O for Hg^0 adsorption over metal oxides sorbent was ascribed to the competitive adsorption [4, 57]. Hence, similar desorption experiments to those described in section 3.4.3 were carried out to verify the competitive adsorption between H_2O and Hg^0. As shown in Fig. 14, a high spike of Hg^0 was observed after cutting off Hg^0 and adding 8% H_2O at the same time due to the desorption of surface adsorbed mercury. This demonstrates that H_2O has strong competitive adsorption with Hg^0 for the same active sites on 0.5Fe1ATT sorbent.

In addition, the Hg^0 removal performance over 0.5Fe1ATT under the atmosphere of O_2, SO_2, NO and H_2O was also tested as shown in Fig. 12. It can be seen that the average Hg^0 removal efficiency in 90 min in the co-existence of 5% O_2, 1000 ppm SO_2, 500 ppm NO and 8% H_2O was 87.5%, which was much higher than that in the presence of 5% O_2, 1000 ppm SO_2, and 8% H_2O separately. The improvement of the Hg^0 removal performance can be ascribed to the beneficial effect of NO, which has been verified in the section 3.4.2. Hence, the 0.5Fe1ATT has the potential to be used as a mercury adsorbent due to its excellent Hg^0 removal performance under the condition of 5% O_2+1000 ppm SO_2+500 ppm NO+8% H_2O.

3.5 Future application perspective

This work is a basic research study focused on understanding the behavior of magnetic sorbents for the control of Hg^0 from the coal-fired boiler flue gases. However, to take full advantage of their characteristics and performance in industrial applications, it will be necessary to improve the basic and applied feature in future work. One is that the acid activation of attapulgite, which will improve structure, physic-chemical, textural and surface properties [64, 65]. The second is the introduction of more active materials, such as halides (Cl, Br, I) and/or metal (Mn, Cu, Co) oxides, which are in favour of greatly enhancing the mercury retention ability. The third one is the evaluation of the lifetime of the sorbent, as well as the regeneration ability. Several regeneration methods investigated by previous studies for the magnetic sorbents, such as Co-MF sorbent [19], $Fe_{3-x}Mn_xO_4$/CNF sorbent [16], and $(Fe_{3-x}Mn_x)_{1-\delta}O_4$ sorbent [66], including the thermal process method [19] and water washing method [16] shall be be considered in the future work of this study.

4 Conclusion

The magnetic xFe1ATT composites were successfully synthesized by the co-precipitation method. The 0.5Fe1ATT sorbent has a satisfactory saturated magnetization, which makes it possible to separate the sorbent from the fly ash for safe disposal of the adsorbed mercury and the regeneration of the sorbent for recycling. O_2 and NO could enhance the Hg^0 removal performance over 0.5Fe1ATT sorbent, while SO_2 and H_2O played an inhibitive role in Hg^0 removal. The inhibition of SO_2 on Hg^0

removal capability could be significantly alleviated by the presence of NO in the flue gas. H_2O competed with Hg^0 for active sites and hence reduced the Hg^0 adsorption ability of the sorbent. This study reveals the possibility of using 0.5Fe1ATT composite as a magnetic sorbent for effective Hg^0 removal, and provides fundamental information about the effects of individual flue gas components on Hg^0 adsorption. Such knowledge is of importance for industrial applications of 0.5Fe1ATT sorbent in coal-fired boilers. Further study should focus on improving the Hg^0 removal performance of the sorbent and evaluating the regeneration of the sorbent.

Acknowledgements

References

(1) Rallo, M.; Lopez-Anton, M. A.; Contreras, M. L.; et al. Mercury policy and regulations for coal-fired power plants. *Environ. Sci. Pollut. Res.* **2012,** *19* (4), 1084-1096.

(2) Yang, J.; Ma, S.; Zhao, Y.; et al. Elemental mercury removal from flue gas over TiO2 catalyst in an internal-illuminated honeycomb photoreactor. *Ind. Eng. Chem. Res.* **2018,** *57* (51), 17348-17355.

(3) Streets, D. G.; Horowitz, H. M.; Jacob, D. J.; et al. Total mercury released to the environment by human activities. *Environ. Sci. Technol.* **2017,** *51* (11), 5969-5977.

(4) Li, H.; Li, Y.; Wu, C.; et al. Oxidation and capture of elemental mercury over SiO2–TiO2–V2O5 catalysts in simulated low-rank coal combustion flue gas. *Chem. Eng. J.* **2011,** *169* (1), 186-193.

(5) Li, J.; Yan, N.; Qu, Z.; et al. Catalytic oxidation of elemental mercury over the modified catalyst Mn/alpha-Al2O3 at lower temperatures. *Environ. Sci. Technol.* **2010,** *44* (1), 426-431.

(6) Liu, H.; Zhao, Y.; Zhou, Y.; et al. Removal of gaseous elemental mercury by modified diatomite. *Sci. Total Environ.* **2019,** *652*, 651-659.

(7) Wilcox, J.; Rupp, E.; Ying, S.; et al. Mercury adsorption and oxidation in coal combustion and gasification processes. *Int. J. Coal Geol.* **2012,** *90-91*, 4-20.

(8) Dong, L.; Xie, J.; Fan, G.; et al. Experimental and theoretical analysis of element mercury adsorption on Fe3O4/Ag composites. *Korean J. Chem. Eng.* **2017,** *34* (11), 2861-2869.

(9) Yang, J.; Zhao, Y.; Zhang, S.; et al. Mercury removal from flue gas by magnetospheres present in fly ash: Role of iron species and modification by HF. *Fuel Process. Technol.* **2017,** *167*, 263-270.

(10) Gao, W.; Liu, Q.; Wu, C.; et al. Kinetics of mercury oxidation in the presence of hydrochloric acid and oxygen over a commercial SCR catalyst. *Chem. Eng. J.* **2013,** *220* (11), 53-60.

(11) Yang, Z.; Li, H.; Liu, X.; et al. Promotional effect of CuO loading on the catalytic activity and SO2 resistance of MnOx/TiO2 catalyst for simultaneous NO reduction and Hg0 oxidation. *Fuel* **2018,** *227*, 79-88.

(12) Li, H.; Zhu, W.; Yang, J.; et al. Sulfur abundant S/FeS2 for efficient removal of mercury from coal-fired power plants. *Fuel* **2018,** *232*, 476-484.

(13) Zhao, H.; Yang, G.; Gao, X.; et al. Hg0 capture over CoMoS/γ-Al2O3 with MoS2 nanosheets at low temperatures. *Environ. Sci. Technol.* **2016,** *50* (2), 1056-1064.

(14) Zhang, L.; Zhuo, Y.; Du, W.; et al. Hg0 removal characteristics of noncarbon sorbents in a fixed-bed reactor. *Ind. Eng. Chem. Res.* **2012,** *51* (14), 5292-5298.

(15) Ghorishi, B. G.; Singer, C. F.; Jozewicz, W. S.; et al. Simultaneous control of Hg0, SO2, and NOx by novel oxidized calcium-based sorbents. *J. Air Waste Manage. Assoc.* **2002,** *52* (3), 273-278.

(16) Yang, J.; Zhao, Y.; Liang, S.; et al. Magnetic iron–manganese binary oxide supported on carbon nanofiber (Fe3−xMnxO4/CNF) for efficient removal of Hg0 from coal combustion flue gas. *Chem. Eng. J.* **2018,** *334*, 216-224.

(17) Cao, T.; Li, Z.; Xiong, Y.; et al. Silica-silver nanocomposites as regenerable sorbents for Hg0 removal from flue gases. *Environ. Sci. Technol.* **2017,** *51* (20), 11909-11917.

(18) Yang, J.; Zhu, W.; Qu, W.; et al. Selenium functionalized metal–organic framework MIL-101 for efficient and permanent sequestration of mercury. *Environ. Sci. Technol.* **2019,** *53* (4), 2260-2268.

(19) Yang, J.; Zhao, Y.; Zhang, J.; et al. Regenerable cobalt oxide loaded magnetosphere catalyst from fly ash for mercury removal in coal combustion flue gas. *Environ. Sci. Technol.* **2014,** *48* (24), 14837-14843.

(20) Sun, H.; Zhao, S.; Ma, Y.; et al. Effective and regenerable Ag/4A zeolite nanocomposite for Hg0 removal from natural gas. *J. Alloys Compd.* **2018,** *762*, 520-527.

(21) Ma, Y.; Mu, B.; Zhang, X.; et al. Graphene enhanced Mn-Ce binary metal oxides for catalytic oxidation and adsorption of elemental mercury from coal-fired flue gas. *Chem. Eng. J.* **2019,** *358*, 1499-1506.

(22) Li, J.; Yan, N.; Qu, Z.; et al. Catalytic oxidation of elemental mercury over the modified catalyst Mn/alpha-Al2O3 at lower temperatures. *Environ. Sci. Technol.* **2010,** *44* (1), 426-31.

(23) He, J.; Reddy, G. K.; Thiel, S. W.; et al. Ceria-modified manganese oxide/titania materials for removal of elemental and oxidized mercury from flue gas. *J. Phys. Chem. C* **2011,** *115* (49), 24300–24309.

(24) Tan, Z.; Su, S.; Qiu, J.; et al. Preparation and characterization of Fe2O3–SiO2 composite and its effect on elemental mercury removal. *Chem. Eng. J.* **2012,** *195-196*, 218-225.

(25) Zhao, B.; Yi, H.; Tang, X.; et al. Using CuO-MnOx/AC-H as catalyst for simultaneous removal of Hg0 and NO from coal-fired flue gas. *J. Hazard. Mater.* **2019,** *364*, 700-709.

(26) Zhu, C.; Wang, X.; Huang, Q.; et al. Removal of gaseous carbon bisulfide using dielectric barrier discharge plasmas combined with TiO2 coated attapulgite catalyst. *Chem. Eng. J.* **2013,** *225*, 567-573.

(27) Li, X.; Yin, Y.; Yao, C.; et al. La1−xCexMnO3/attapulgite nanocomposites as catalysts for NO reduction with NH3 at low temperature. *Particuology* **2016,** *26*, 66-72.

(28) Murray, H. H.. Traditional and new applications for kaolin, smectite, and palygorskite: a general overview. *Appl. Clay Sci.* **2000,** *17* (5), 207-221.

(29) Xue, A.; Zhou, S.; Zhao, Y.; et al. Effective NH2-grafting on attapulgite surfaces for adsorption of reactive dyes. *J. Hazard. Mater.* **2011,** *194*, 7-14.

(30) Wang, W.; Wang, A.. Recent progress in dispersion of palygorskite crystal bundles for nanocomposites. *Appl. Clay Sci.* **2016,** *119*, 18-30.

(31) Li, X.; Ni, C.; Yao, C.; et al. Development of attapulgite/Ce1−xZrxO2 nanocomposite as catalyst for the degradation of methylene blue. *Appl. Catal., B* **2012,** *117-118*, 118-124.

(32) Wu, X.; Zhu, W.; Zhang, X.; et al. Catalytic deposition of nanocarbon onto palygorskite and its adsorption of phenol. *Appl. Clay Sci.* **2011,** *52* (4), 400-406.

(33) Xie, A.; Zhou, X.; Huang, X.; et al. Cerium-loaded MnOx/attapulgite catalyst for the low-temperature NH3-selective catalytic reduction. *Ind. Eng. Chem. Res.* **2017,** *49*, 230-241.

(34) Li, X.; Yan, X.; Zuo, S.; et al. Construction of LaFe1−xMnxO3/attapulgite nanocomposite for photo-SCR of NOx at low temperature. *Chem. Eng. J.* **2017,** *320*, 211-221.

(35) Zhou, X.; Huang, X.; Xie, A.; et al. V2O5-decorated Mn-Fe/attapulgite catalyst with high SO2 tolerance for SCR of NOx with NH3 at low temperature. *Chem. Eng. J.* **2017,** *326*, 1074-1085.

(36) Liu, H.; Yang, J.; Tian, C.; et al. Mercury removal from coal combustion flue gas by modified palygorskite adsorbents. *Appl. Clay Sci.* **2017,** *147*, 36-43.

(37) Yang, J.; Zhao, Y.; Ma, S.; et al. Mercury removal by magnetic biochar derived from simultaneous activation and magnetization of sawdust. *Environ. Sci. Technol.* **2016,** *50* (21), 12040-12047.

(38) Lu, Z.; Hao, Z.; Wang, J.; et al. Efficient removal of europium from aqueous solutions using attapulgite-iron oxide magnetic composites. *Ind. Eng. Chem. Res.* **2016,** *34*, 374-381.

(39) Zhang, J.; Zhang, L.; Zhou, S.; et al. Magnetically separable attapulgite−TiO2−FexOy composites with superior activity towards photodegradation of methyl orange under visible light radiation. *Ind. Eng. Chem. Res.* **2014,** *20* (5), 3884-3889.

(40) Dong, J.; Xu, Z.; Kuznicki, S. M.. Mercury Removal from flue gases by novel regenerable magnetic nanocomposite sorbents. *Environ. Sci. Technol.* **2009,** *43* (9), 3266-3271.

(41) Kim, Y. H.; Sim, B.; Choi, H. J.. Fabrication of magnetite-coated attapulgite magnetic composite nanoparticles and their magnetorheology. *Colloids Surf., A* **2016,** *507*, 103-109.

(42) Xu, J.; Li, W.; Yin, Q.; et al. Direct electrochemistry of Cytochrome c on natural nano-attapulgite clay modified electrode and its electrocatalytic reduction for H2O2. *Electrochim. Acta* **2007,** *52* (11), 3601-3606.

(43) Li, B.; Li, L.; Zhang, Q.; et al. Attapulgite as natural catalyst for glucose isomerization to fructose in water. *Catal. Commun.* **2017,** *99*, 20-24.

(44) Xu, J.; Zhu, Y.. Monodisperse Fe3O4 and γ-Fe2O3 Magnetic mesoporous microspheres as anode materials for lithium-ion batteries. *ACS Appl. Mater. Interfaces* **2012,** *4* (9), 4752-4757.

(45) Zhang, S.; Zhao, Y.; Yang, J.; et al. Fe-modified MnOx/TiO2 as the SCR catalyst for simultaneous removal of NO and mercury from coal combustion flue gas. *Chem. Eng. J.* **2018,** *348*, 618-629.

(46) Reddy, B. M.; Chowdhury, B.; Smirniotis, P. G.. An XPS study of the dispersion of MoO3 on TiO2–ZrO2, TiO2–SiO2, TiO2–Al2O3, SiO2–ZrO2, and SiO2–TiO2–ZrO2 mixed oxides. *Appl. Catal., A* **2001,** *211* (1), 19-30.

(47) Brovelli, F.; Rivas, B. L.; Bernède, J. C.. Electropolymerization of heteroarylene azomethines. *J. Chil. Chem. Soc.*, **2005,** *50*, 597-602.

(48) Chen, W.; Zhang, Z.; Bao, W.; et al. Hierarchical mesoporous γ-Fe2O3/carbon nanocomposites derived from metal organic frameworks as a cathode electrocatalyst for rechargeable Li-O2 batteries. *Electrochim. Acta* **2014,** *134*, 293-301.

(49) Zhao, Y.; Xue, F.; Ma, T.. Experimental study on Hg0 removal by diperiodatocuprate (III) coordination ion solution. *Fuel Process. Technol.* **2013,** *106*, 468-473.

(50) Baikousi, M.; Bourlinos, A. B.; Douvalis, A.; et al. Synthesis and characterization of γ-Fe2O3/carbon hybrids and their application in removal of hexavalent chromium ions from aqueous solutions. *Langmuir* **2012,** *28* (8), 3918-3930.

(51) Chen, D.; Zhao, S.; Qu, Z.; et al. Cu-BTC as a novel material for elemental mercury removal from sintering gas. *Fuel* **2018,** *217*, 297-305.

(52) Li, H.; Wang, Y.; Wang, S.; et al. Removal of elemental mercury in flue gas at lower temperatures over Mn-Ce based materials prepared by co-precipitation. *Fuel* **2017,** *208*, 576-586.

(53) Zhou, Z.; Liu, X.; Zhao, B.; et al. Elemental mercury oxidation over manganese-based perovskite-type catalyst at low temperature. *Chem. Eng. J.* **2016,** *288*, 701-710.

(54) Zeng, X.; Xu, Y.; Zhang, B.; et al. Elemental mercury adsorption and regeneration performance of sorbents FeMnOx enhanced via non-thermal plasma. *Chem. Eng. J.* **2017,** *309*, 503-512.

(55) Yang, B.; Li, Z.; Huang, Q.; et al. Synergetic removal of elemental mercury and NO over TiCe0.25Sn0.25Ox catalysts from flue gas: Performance and mechanism study. *Chem. Eng. J.* **2019,** *360*, 990-1002.

(56) Li, Y.; Murphy, P. D.; Wu, C.; et al. Development of silica/vanadia/titania catalysts for removal of elemental mercury from coal-combustion flue gas. *Environ. Sci. Technol.* **2008,** *42* (14), 5304-5309.

(57) Li, H.; Wu, C.; Li, Y.; et al. Role of flue gas components in mercury oxidation over TiO2 supported MnOx-CeO2 mixed-oxide at low temperature. *J. Hazard. Mater.* **2012,** *243*, 117-123.

(58) Wang, P.; Hu, S.; Xiang, J.; et al. Analysis of mercury species over CuO–MnO2–Fe2O3/γ-Al2O3 catalysts by thermal desorption. *Proc. Combust. Inst.* **2015,** *35* (3), 2847-2853.

(59) Chen, G.; Zhang, D.; Zhang, A.; et al. CrOx–MnOx–TiO2 adsorbent with high resistance to SO2 poisoning for Hg0 removal at low temperature. *Ind. Eng. Chem. Res.* **2017,** *55*, 119-127.

(60) Li, H.; Wu, C.; Li, Y.; et al. Impact of SO2 on elemental mercury oxidation over CeO2–TiO2 catalyst. *Chem. Eng. J.* **2013,** *219*, 319-326.

(61) Yang, W.; Liu, Y.; Wang, Q.; et al. Removal of elemental mercury from flue gas using wheat straw chars modified by Mn-Ce mixed oxides with ultrasonic-assisted impregnation. *Chem. Eng. J.* **2017,** *326*, 169-181.

(62) Xu, W.; Tong, L.; Qi, H.; et al. Effect of Flue Gas Components on Hg0 Oxidation over Fe/HZSM-5 Catalyst. *Ind. Eng. Chem. Res.* **2015,** *54* (1), 146-152..

(63) Zhao, Y.; Hao, R.; Zhang, P.; et al. An integrative process for Hg0 removal using vaporized H2O2/Na2S2O8. *Fuel* **2014,** *136*, 113-121.

(64) Abdul-Latif, N.; Weaver, C. E. Kinetics of Acid-Dissolution of Palygorskite (Attapulgite) and Sepiolite. *Clays Clay Miner.* **1969,** *17* (3), 169-178.

(65) Pushpaletha, P.; Lalithambika, M. Modified attapulgite: An efficient solid acid catalyst for acetylation of alcohols using acetic acid. *Appl. Clay Sci.* **2011,** *51* (4), 424-430.

(66) Yang, S.; Yan, N.; Guo, Y.; et al. Gaseous Elemental Mercury Capture from Flue Gas Using Magnetic Nanosized (Fe3-xMnx)1-δO4. *Environ. Sci. Technol.* **2011,** *45* (4), 1540-1546.